A deformation gradient tensor and strain tensors for atomistic simulations

Modelling Simul. Mater. Sci. Eng. **16** (2008) 015001 (17pp) doi:10.1088/0965-0393/16/1/015001

A deformation gradient tensor and strain tensors for atomistic simulations

P M Gullett[1], M F Horstemeyer[1], M I Baskes[2] and H Fang[3]

[1] Mississippi State University, Center for Advanced Vehicular Systems, MS 39762, USA
[2] Los Alamos National Laboratory, Los Alamos, NM 87545, USA
[3] University of North Carolina at Charlotte, Charlotte NC 28223, USA

E-mail: pmgullett@cee.msstate.edu

Received 17 November 2006, in final form 2 October 2007
Published 13 December 2007
Online at stacks.iop.org/MSMSE/16/015001

Abstract

A kinematical algorithm is proposed for the construction of strain tensors from atomistic simulation data. Local strain tensors such as the Almansi and Green strain tensors suitable for use in large deformation molecular dynamics/statics simulations are computed directly from a discrete form of the deformation gradient. The discrete, incremental form of the deformation gradient emerges from a weighted least squares minimization that includes a length scale relating the distance from the atom in question with a particular radius. This region defines the nonlocal domain of the strain at that atom. The local atomic strain tensors are then computed using continuum definitions in terms of the deformation gradient. The results of molecular dynamics simulations are presented that compare the Almansi and Green strain tensors under inhomogeneous deformation and indicate that the small-strain approximation should not be used to determine large atomic strains.

(Some figures in this article are in colour only in the electronic version)

This paper presents a method for computing a deformation gradient and strain tensors from incremental atomic motions generated by atomistic simulations that are consistent with strain tensors defined in the continuum mechanics framework. Strain tensors are the primary measure of local deformations used in continuum analysis. Unlike displacement, strain is not a measurable quantity, but is computed from a definition that relies on the gradient of a continuous displacement field. Because atomistic simulations provide atomic positions at discrete time intervals, the definition of local deformation in terms of strain is troublesome, and thus correlating with larger scale continuum results is difficult.

Many engineering problems involve physical phenomena at multiple length scales. Consequently, a significant amount of research has been devoted to the development of simulation tools that provide a link between atomic scale and continuum theories. See Liu *et al* [1] for a review of multiscale methods. Multiscale simulation techniques typically fall into two categories: concurrent and hierarchical. Concurrent methods, e.g. the

quasicontinuum method of Tadmore *et al* [2], seek to incorporate aspects of various size scale phenomena in a single simulation. Such techniques are particularly useful for simulating the behavior of structures with multiple length scale geometries, such as thin films and nanotubes, as well as material fracture. In contrast, hierarchical techniques seek to identify and quantify cause-effect relationships at lower scales and incorporate them into macroscale level models. See for example Horstemeyer [3, 4].

Among the challenges for hierarchical models is the need to provide a common measure of deformation between atomic scale simulations and the continuum framework. Deformation measures typical in molecular dynamics simulations such as centro-symmetry present in Kelchner *et al* [5] and the slip vector by Zimmerman *et al* [6] have proved to be powerful tools for identifying lattice distortion and the formation of dislocation structures, but correlation in the context of hierarchical modeling is difficult because these measures are not utilized in the continuum framework.

This work seeks to provide a simple means to interpret time histories of atomic positions generated by molecular dynamics simulations in a manner analogous to and consistent with the usual continuum mechanical framework through the development of a local atomic deformation gradient from which strain tensors may be computed. Because strain is fundamentally a continuum quantity, its computation from atomic displacement data requires either interpolation of a continuous displacement field or a discretization of the gradient operator. In this work we take the latter approach.

At least two methods for computation of strain tensors have been proposed in the literature. Mott *et al* [7] presented a local atomic strain measure for three-dimensional, disordered systems (e.g. glass). In this approach, the atomic displacements are interpolated using a continuous, piecewise-linear basis formed by a Delaunay tessellation of the atomic positions. The displacement at any point in a tetrahedron is a linear function of the displacements of the atoms at its vertices, and the deformation gradient is constant. The local atomic deformation gradient is then defined as a weighted average of the deformation gradients of adjacent tetrahedrons. Strain tensors are then computed directly from their definitions in terms of the deformation gradient. While strain tensors constructed utilizing this approach are applicable to finite deformations (e.g. Ward *et al* [8]), the method can be computationally expensive due to the required geometric decomposition; thus, it is generally not recommended for simulations that include significant plastic flow.

Falk [9] constructed a local atomic strain tensor using the small-strain definition. In this approach, a locally constant atomic strain tensor is computed based on the relative motion of an atom and its nearest neighbors. Although this formulation is straightforward, the method suffers because rigid body rotations appear as fictitious shear strains and finite strains are not represented accurately when using this strain definition.

We propose an atomic strain tensor that is based on the definition of a discrete equivalent to the continuum deformation gradient that accounts for the relative motion of an atom and its neighbors in a nonlocal fashion. The approach, based on the idea presented by Horstemeyer [10], is computationally efficient because the deformation gradient arises from an optimization procedure that does not rely on a geometric decomposition. The strain tensors are computed directly from the deformation gradient and are appropriate for general finite, multi-axial deformation states. The direct computation of the deformation gradient and strain tensors make the approach useful for evaluation of continuum models [11], development of microstructure and mechanical property relationships, identification of dislocations and disclinations, as well as for quantification of plastic spin and strain gradients.

Notation is standard, with Cartesian tensors being distinguished from scalars in bold font. In this work the term discrete is used when addressing the discontinuous nature of a body

composed of atoms, and incremental refers to the temporally discrete sequence of atomic configurations generated by atomistic simulations.

1. Strain formulation

In this section we briefly consider the continuum deformation gradient, introduce a discrete version of the deformation gradient, and finally present the strain tensors.

1.1. Continuum deformation gradient

As motivation for a discrete deformation gradient, we first consider the continuum mechanics deformation gradient. For simplicity, we assume a fixed Cartesian coordinate system and a continuous body composed of particles that are identified by the position vectors that specify their place in the initial configuration. A motion, χ, maps a particle from its initial position $\boldsymbol{X}$ in the reference configuration Ω_0, to its position $\boldsymbol{x}$ in the current configuration Ω_1 and is represented by

$$\boldsymbol{x} = \chi(\boldsymbol{X}). \tag{1}$$

Assuming sufficient continuity, the local deformation at $\boldsymbol{X}$ is characterized as the gradient of the motion, which is a second order, two-point tensor defined as

$$\boldsymbol{F} \equiv \frac{\partial \chi}{\partial \boldsymbol{X}} = \frac{\partial \boldsymbol{x}}{\partial \boldsymbol{X}}. \tag{2}$$

The deformation of an infinitesimal segment at point in the reference configuration is given by

$$\mathrm{d}\boldsymbol{x} = \chi(\boldsymbol{X} + \mathrm{d}\boldsymbol{X}) - \chi(\boldsymbol{X}). \tag{3}$$

Expanding equation (3) in a Taylor series and considering only first order terms yields an approximation for $\mathrm{d}\boldsymbol{x}$:

$$\mathrm{d}\boldsymbol{x} = \chi(\boldsymbol{X}) + \nabla\chi(\boldsymbol{X}) \cdot \mathrm{d}\boldsymbol{X} + o(\mathrm{d}\boldsymbol{X}) - \chi(\boldsymbol{X}), \tag{4}$$

$$\mathrm{d}\boldsymbol{x} \approx \nabla\chi(\boldsymbol{X}) \cdot \mathrm{d}\boldsymbol{X}. \tag{5}$$

In equation (4), the notation $o(\cdot)$ takes the usual meaning of a term that approaches zero faster than its argument $(\cdot)$. Substituting $\boldsymbol{F}$ from equation (2) into equation (5) results in

$$\mathrm{d}\boldsymbol{x} \approx \boldsymbol{F} \cdot \mathrm{d}\boldsymbol{X}. \tag{6}$$

Similarly, because of regularity assumptions the reverse mapping is given by

$$\boldsymbol{F}^{-1}\mathrm{d}\boldsymbol{x} \approx \mathrm{d}\boldsymbol{X}. \tag{7}$$

Thus, the deformation gradient $\boldsymbol{F}$ maps an arbitrary, infinitesimal vector $\mathrm{d}\boldsymbol{X}$ at $\boldsymbol{X}$ in the reference configuration to $\mathrm{d}\boldsymbol{x}$ at $\boldsymbol{x}$ in the current configuration.

1.2. Strain tensors

Strain is a measure of the deformation of a body with respect to a reference configuration. While many strain measures are possible, e.g. see [12], we consider two common measures. From equation (6), the change in the squared length of the vector $\mathrm{d}\boldsymbol{X}$ is given by

$$\mathrm{d}\boldsymbol{x} \cdot \mathrm{d}\boldsymbol{x} - \mathrm{d}\boldsymbol{X} \cdot \mathrm{d}\boldsymbol{X} = \mathrm{d}\boldsymbol{X} \cdot (\boldsymbol{F}^{\mathrm{T}}\boldsymbol{F} - \boldsymbol{I})\,\mathrm{d}\boldsymbol{X}. \tag{8}$$

Here, the deformation is characterized entirely in terms of the reference configuration by the dimensionless, symmetric second order tensor

$$\boldsymbol{F}^{\mathrm{T}}\boldsymbol{F} - \boldsymbol{I}. \tag{9}$$

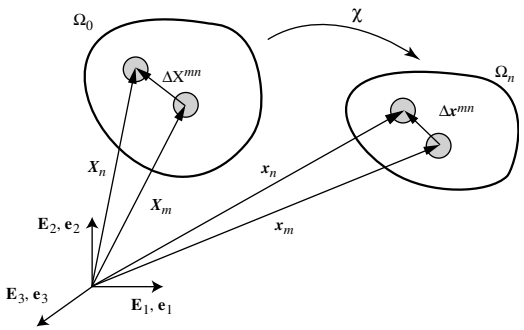

Figure 1. General motion in the neighborhood of a discrete atomic particle. The areas labeled Ω_0 and Ω_n represent the atomic system in reference and current configurations. The shaded circles represent discrete atomic positions that are specified with position vectors $\boldsymbol{X}^m$ and $\boldsymbol{x}^m$ in the reference and current configurations respectively.

The Lagrangian or Green strain tensor, $\boldsymbol{E}$, is defined with respect to reference coordinates in terms of this quantity as

$$\boldsymbol{E} = \tfrac{1}{2}(\boldsymbol{F}^{\mathrm{T}}\boldsymbol{F} - \boldsymbol{I}). \tag{10}$$

The representation of strain, defined in terms of the Eulerian coordinates is given by,

$$\boldsymbol{\varepsilon} = \tfrac{1}{2}(\boldsymbol{I} - (\boldsymbol{F}\boldsymbol{F}^{\mathrm{T}})^{-1}). \tag{11}$$

The Lagrangian Green strain is particularly suitable for problems of elasticity because there is usually an undeformed state to which the body is elastically unloaded while the Eulerian–Almansi strain, used for example in the interpretation of experimental interferometric Moiré data, may be preferable when the presence of dislocations in the distorted lattice prevent a return to the reference configuration.

1.3. Discrete deformation gradient

The absence of a continuous displacement field prevents computation of the deformation gradient (see equation (2)) directly from atomistic simulation data. In this subsection, we propose a discrete deformation gradient that emerges from an optimization of a discrete form of equation (6).

In this discussion, a generic time increment under consideration is assumed to be such that $t \in [t_0, t_l]$. For simplicity, the atomic configurations under consideration at $t = t_0$ and $t = t_l$ are denoted by Ω_0 and Ω_l. The deformation gradient mapping between these configurations is $\boldsymbol{F}_l$. Note that although $\boldsymbol{F}_l$ is the deformation gradient with respect to the global reference configuration, this development is not inherently restricted to any particular choice of reference configuration. In fact, the following procedure could be used to construct an 'incremental' deformation gradient between any two configurations Ω_l and Ω_i where $t_i \in [t_0, t_{l-1}]$.

Consider an atomic system shown in figure 1. The deformation in the neighborhood of atom m is characterized by the changes in the relative position of its neighbors. Atom m is located at the position $\boldsymbol{X}^m$ in configuration Ω_0 and position $\boldsymbol{x}^m$ in configuration Ω_l. The relative position of neighboring atom n is given by the vector

$$\Delta\boldsymbol{X}^{mn} = \boldsymbol{X}^n - \boldsymbol{X}^m \tag{12}$$

in configuration Ω_0 and by

$$\Delta\boldsymbol{x}^{mn} = \boldsymbol{x}^n - \boldsymbol{x}^m \tag{13}$$

in configuration Ω_l. In equations (12) and (13) the superscripts denote atom numbers, and the vectors $\Delta \boldsymbol{X}^{mn}$ and $\Delta \boldsymbol{x}^{mn}$ connect atom m to its neighbors n. There exists a unique linear mapping that transforms the relative position vector $\Delta \boldsymbol{X}^{mn}$ to $\Delta \boldsymbol{x}^{mn}$:

$$\Delta \boldsymbol{x}^{mn} = \boldsymbol{F}^m \cdot \Delta \boldsymbol{X}^{mn}, \tag{14}$$

where $\boldsymbol{F}^m$ is the value of the deformation gradient at atom m. Here, equation (14) defines the operation of the discrete deformation gradient at atom m in a manner analogous to the continuum deformation gradient of equation (6) in that it maps a vector in the reference configuration to a vector in the current configuration. Writing equation (6) for atom m and each of its neighbors leads to a system of linear equations that, because of the freedom of the atomic motion, cannot generally be satisfied by a single mapping $\boldsymbol{F}^m$. For this reason, an optimal local deformation gradient, $\hat{\boldsymbol{F}}^m$, is sought. We measure the mapping error between atom m and a single neighbor n as the ℓ^2 norm of the difference between the $\Delta \boldsymbol{x}^{mn}$ and $\hat{\boldsymbol{F}}^m \cdot \Delta \boldsymbol{X}^{mn}$:

$$\phi^{mn} = (\Delta \boldsymbol{x}^{mn} - \hat{\boldsymbol{F}}^m \Delta \boldsymbol{X}^{mn})^{\mathrm{T}} (\Delta \boldsymbol{x}^{mn} - \hat{\boldsymbol{F}}^m \Delta \boldsymbol{X}^{mn}). \tag{15}$$

Thus, the weighted least squares error among the neighbors of m is given by

$$\phi^m = \sum_{n=1}^{N} (\Delta \boldsymbol{x}^{mn} - \hat{\boldsymbol{F}}^m \Delta \boldsymbol{X}^{mn})^{\mathrm{T}} (\Delta \boldsymbol{x}^{mn} - \hat{\boldsymbol{F}}^m \Delta \boldsymbol{X}^{mn}) w_n, \tag{16}$$

where N is the number of neighboring atoms, and w_n is a weight factor.

In this formulation, we are primarily concerned with local deformation at individual atoms in systems subjected to inhomogeneous deformations; thus the local deformation gradient is computed without extension of the mapping error to the bulk. The optimal local deformation gradient $\hat{\boldsymbol{F}}^m$, in a least squares sense, is obtained by minimizing ϕ^m with respect to the components of $\hat{\boldsymbol{F}}$,

$$\frac{\partial \phi^m}{\partial \hat{F}_{ij}} = \sum_n (-2\Delta x_i^{mn} \Delta X_j^{mn} + 2\Delta X_j^{mn} \hat{F}_{ik} \Delta X_k^{mn}) w_n. \tag{17}$$

Setting equation (17) equal to zero and solving for the components of $\hat{\boldsymbol{F}}$:

$$\sum_n (-\Delta x_i^{mn} \Delta X_j^{mn} + \hat{F}_{ik} \Delta X_k^{mn} \Delta X_j^{mn}) w_n = 0, \tag{18}$$

$$\hat{F}_{ik} \sum_n \Delta X_k^{mn} \Delta X_j^{mn} w_n = \sum_n \Delta x_i^{mn} \Delta X_j^{mn} w_n, \tag{19}$$

which in matrix notation is given by

$$\hat{\boldsymbol{F}} \sum_n \Delta \boldsymbol{X}^{mn} \Delta \boldsymbol{X}^{mn\mathrm{T}} w_n = \sum_n \Delta \boldsymbol{x}^{mn} \Delta \boldsymbol{X}^{mn\mathrm{T}} w_n. \tag{20}$$

This linear system of equations that can be written as

$$\hat{\boldsymbol{F}} \boldsymbol{D} = \boldsymbol{A}. \tag{21}$$

where $\boldsymbol{D}$ and $\boldsymbol{A}$ are 3×3 matrices

$$\boldsymbol{D} = \sum_n \Delta \boldsymbol{X}^{mn} \Delta \boldsymbol{X}^{mn\mathrm{T}} w_n, \tag{22}$$

and

$$\boldsymbol{A} = \sum_n \Delta \boldsymbol{x}^{mn} \Delta \boldsymbol{X}^{mn\mathrm{T}} w_n. \tag{23}$$

Provided that $\boldsymbol{D}$ was formed from a minimum of three noncoplanar nearest neighbors having nonzero weights, the optimal discrete deformation gradient is determined as

$$\hat{\boldsymbol{F}} = \boldsymbol{A}\boldsymbol{D}^{-1}. \tag{24}$$

which is the deformation gradient of Ω_n with respect to Ω_0.

An essential difference between the properties of the discrete deformation gradient defined by equation (14) and the continuum form should be noted. The continuum deformation gradient depends on the existence of a body comprised of a continuous distribution of material and a smooth, differentiable motion. These assumptions engender an integrability condition: that the curl of the deformation gradient vanishes. In the discrete system, only a succession of discrete atomic positions is considered, and while the motion of the atom is assumed to be smooth, no postulation of a smooth motion of a continuous region of space is made. Furthermore, the discrete deformation gradient is not known as a function of spatial position, but only at atomic locations; hence, no integrability conditions, similar to those of the continuum deformation gradient, are required. On the other hand, this procedure determines the local affine deformation that optimally (in a weighted least squares sense) approximates the true motion. This is observed from the fact that if the discrete atomic positions are prescribed by a globally linear motion, such as simple shear, then this method will recover the exact deformation gradient.

1.4. Weight function

The weight function plays an important role in the formulation of the discrete deformation gradient. When forming the deformation gradient at an atom, we generally seek contributions from atoms within a certain proximity and assign the nearest neighbor atoms a stronger influence than those farther away. Thus, weights functions should evaluate to unity for nearest neighbors, and decrease monotonically to zero as a function of the distance between the atoms and its neighbors. Figure 2(*a*) shows cubic spline weight functions with various cutoff distances. By varying the cutoff distance, the nonlocal domain of influence on the deformation gradient computation can be examined.

While the precise form of a monotonically decreasing weight function has little effect on the bulk average results, in some instances it is desirable to choose functions that have a zero spatial gradient (figure 2(*b*)) in order to eliminate the influence of thermal vibrations on the computed strains. In particular, because the choice of reference configuration is essentially arbitrary, deformation gradients can be computed between several intermediate configurations and referenced back to the global reference by multiplying the intermediate gradients (note that this procedure, while strictly true for continuum motions, will not generally yield a final deformation gradient that is identical to the optimized gradient computed by utilizing the current and global reference configurations directly in 24). When the number of intermediate gradients becomes large, thermal vibrations may have a noticeable effect on the computed gradient if weight functions with nonzero spatial gradients are used.

In this paper, weighting factors are computed as follows: neighbors are grouped according to their proximity to the current atom, i.e. first nearest neighbors, second nearest and so forth. Next, weights are assigned to the groups using the cubic spline

$$w(r) = \begin{cases} 1 - 6r^2 + 6r^3 : & r \leqslant \dfrac{1}{2}, \\ 2 - 6r + 6r^2 - 2r^3 : & \dfrac{1}{2} < r < 1.0, \\ 0 : & r \geqslant 1.0, \end{cases} \tag{25}$$

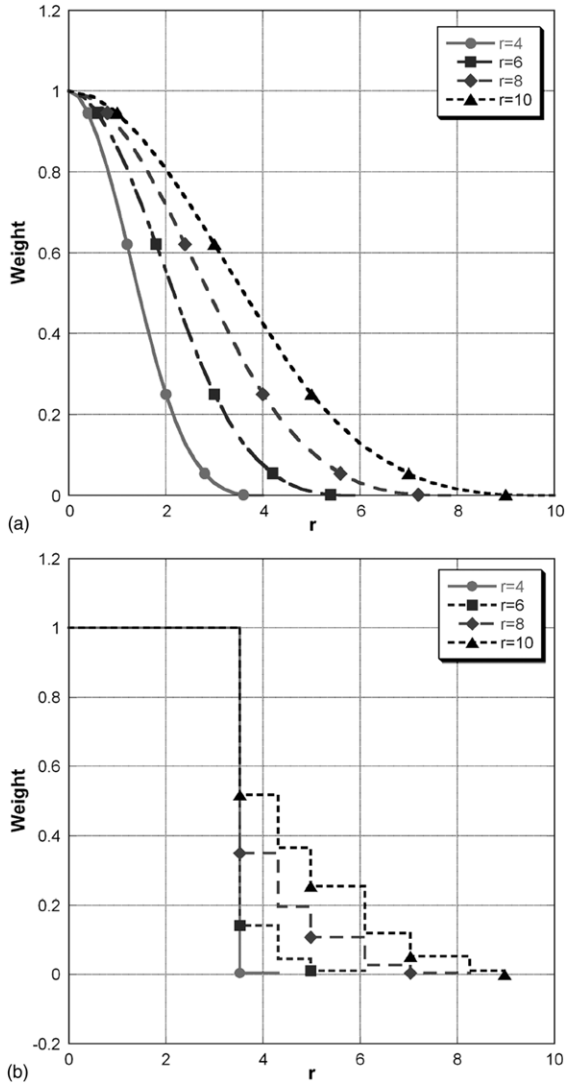

Figure 2. Weight function specification for various cutoff radii by (*a*) cubic splines and (*b*) step functions.

where the value of r for the ith nearest neighbor group is computed as

$$r = (r_{gi} - r_{g1})/r_{\text{cut}}. \tag{26}$$

Here, r_{g1} and r_{gi} are the distances between the current atom and the closest neighbors in the first and ith neighbor groups; r_{cut} is the cutoff radius that specifies the domain over which the weight function is nonzero. The effect of changing the size of the cutoff radius is examined in section 2.

2. Example strain calculation

This simulation provides an example of the computed strain for a block of nickel atoms subjected to fixed-end, simple shear-like boundary conditions. The embedded atom

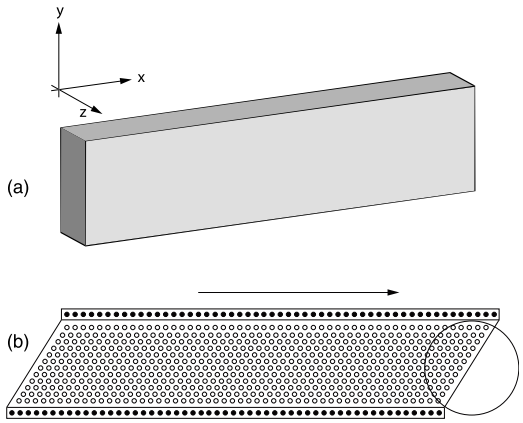

Figure 3. Schematic of the simulation block of atoms in the (*a*) initial configuration and (*b*) at large strain in which the clear circles represent active atoms and the dark circles represent boundary atoms strained configuration. The ends of the system (circled region) must remain planar to satisfy the definition of simple strain. However, during the atomistic simulations the plane typically experiences some perturbation, hence the motion is 'simple shear like.'

method (EAM) potential described by [13, 14] was used to compute atomic motions. The EAM utilizes a pair potential augmented by an effective embedding energy term to account for many-body interactions.

The geometry of the nickel atom block, shown in figure 3(*a*), is 35 Å high, 140 Å long and 14 Å thick. The lattice crystal directions [1 0 0], [0 1 1] and [0 1 $\bar{1}$] correspond to the x, y, and z axes, respectively. The atomic velocities were initialized using a Boltzmann distribution at 300 K, and the system was equilibrated before the shear velocity was applied.

The simple shear-like deformation was achieved by imposing a constant x-direction velocity of $v_x = 0.035\,\text{Å}\,\text{ps}^{-1}$ on the $+y$ surface atoms, while holding the $-y$ surface atoms fixed as indicated in figure 3(*b*). The x and z surfaces were modeled with periodic boundary conditions. The imposed boundary conditions differ from a rigorous continuum description of simple shear in that the x faces are not constrained to remain parallel during the simulation, and the prescribed shear velocity is only applied to the atoms on the $+y$ surface. As will be seen, the equivalence of the actual boundary conditions with those of true simple shear is approximately satisfied until the onset of plastic deformation. A block subjected to a true simple shear motion is described by a spatially constant deformation gradient

$$\boldsymbol{F}(t) = \begin{bmatrix} 1 & v_x t/h & 0 \\ 0 & 1 & 0 \\ 0 & 0 & 1 \end{bmatrix}, \tag{27}$$

where v_x is the velocity of the top surface, t is time and h is the height of the slab. The Almansi and Green strain tensors from this gradient are given by

$$\boldsymbol{\varepsilon}(t) = \frac{1}{2}\begin{bmatrix} 0 & v_x t/h & 0 \\ v_x t/h & -(v_x t/h)^2 & 0 \\ 0 & 0 & 0 \end{bmatrix} \tag{28}$$

and

$$\boldsymbol{E}(t) = \boldsymbol{F}^{\mathrm{T}}\varepsilon\boldsymbol{F} = \frac{1}{2}\begin{bmatrix} 0 & v_x t/h & 0 \\ v_x t/h & (v_x t/h)^2 & 0 \\ 0 & 0 & 0 \end{bmatrix}. \tag{29}$$

For the postulated homogeneous deformation, the shear strain values are identical for the Green and Almansi strain tensors.

A few definitions are now introduced. In the following discussion and figures, the term 'applied strain' refers to a continuum measure of the relative displacement between the top and bottom surfaces of the slab. The magnitude of the 'applied strain' is given by $v_x t/h$. The term 'computed strain' refers to strain tensor values calculated using the optimized local deformation gradient of equation (24) in connection with the Green or Almansi strain definitions in equations (10) and (11). Unless otherwise indicated, the strains were computed using the weight function of equation (25) with a 'cutoff' radius of 8 Å.

Atomic stress was computed using the viral stress definition,

$$\sigma_{ij} = \left\langle \frac{1}{V_\alpha} \sum_\beta F^i_{\alpha\beta} r^j_{\alpha\beta} \right\rangle_\alpha \tag{30}$$

where i and j are indices representing spatial directions, α and β are atom indices, and the notation $\langle\cdot\rangle_\alpha$ represents an average over atoms α. The strain tensors were computed according to equations (10) and (11) using the deformation gradient of equation (24).

2.1. Bulk strain response

The average computed shear strain results are summarized in figure 4. Qualitatively, figure 4(*a*) shows that the average computed Green and Almansi shear strains initially increase at the same rate as the assumed simple shear response until the maximum stress is reached at approximately 6.4% applied strain. After 6.4% applied strain, plasticity initiates via dislocation nucleation and motion, and the average computed Green and Almansi strains begin to differ. The computed Almansi strain increases at a rate that is slightly higher than the applied strain, and the Green strain increases a slightly lower rate.

Figure 4(*b*) shows that during the initial, elastic deformation, the difference between the computed Almansi and Green strains is negligible, averaging 0.23%. This is consistent with the continuum shear strain components in equations (28) and (29). When the system reaches its maximum stress value at 6.4% applied strain, the difference in the Almansi and Green strains jumps to 5.0% and then increases steadily. After 10% applied strain, the difference between the computed Green and Almansi strains continues to increase, but at a lower rate.

The initial deformation of the system is consistent with the Cauchy–Born hypothesis [15] with the motion of the boundary atoms being accommodated through stretching of atomic bonds and the uniform tilting of the initially vertical atomic planes as shown in figures 5(*a*) and (*b*). As expected, before the onset of plastic deformation, the computed Green and Almansi shear strains are consistent with a homogeneous deformation. At 3.0% applied strain, figure 5, the average local computed shears are 3.0% with a standard deviation of 0.6%. As the system approaches its peak stress, the variation in local computed strain increases. At 6.0% applied strain, figure 6, the bulk average computed shear strain is 6.0% with a standard deviation of 0.8%.

The system reaches the peak stress at 6.4% applied strain, and although bulk average computed shear strain is equal to the applied strain, the system undergoes a significant redistribution of deformation. Figure 7 shows that the shear strain is highly localized in the

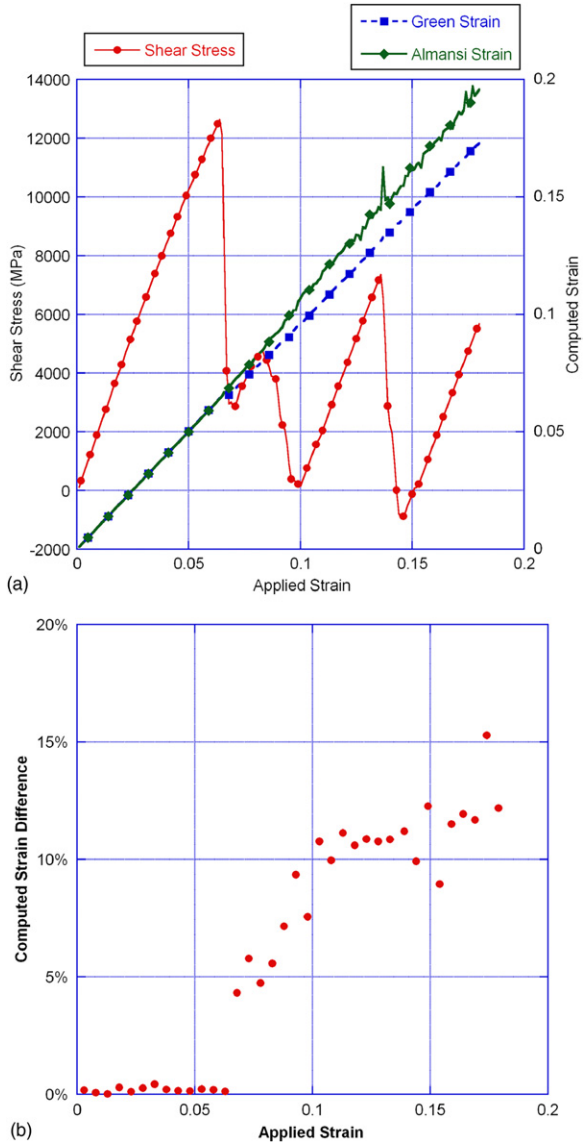

Figure 4. (*a*) The computed bulk average shear stress and the Almansi and Green shear strains are plotted against the applied strain. (*b*) The per cent difference between the average Green and Almansi shear strains are plotted versus applied strain.

(1 0 0) slip planes. Near the dislocation nucleation sites, the strain levels vary from 0% to 20%. Away from the highly strained region, the lattice has uniformly unloaded to approximately 3% strain. This deformation pattern represents a transition from the homogeneous simple shear motion to an inhomogeneous one.

At 7.0% applied strain (figure 8) the deformation is characterized by organization and motion of dislocations concentrated along the (1 0 0), (1 1 1), and ($\bar{1}$ 1 1) crystallographic slip planes. The computed Almansi and Green shear strains provide equivalent results for (1 0 0) slip but differ for (1 1 1) and ($\bar{1}$ 1 1). This difference is consistent with the expected behavior

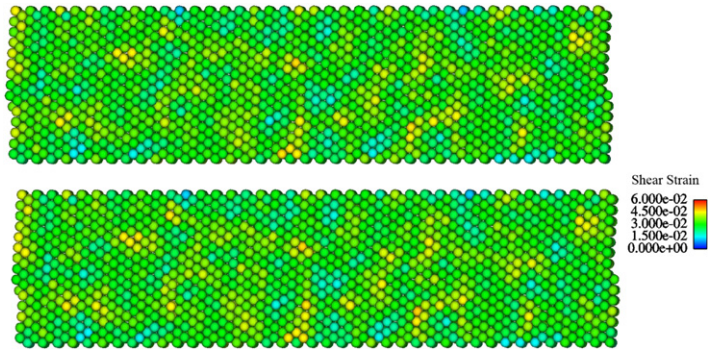

Figure 5. Computed Almansi (top) and Green (bottom) strains at 3.0% applied strain.

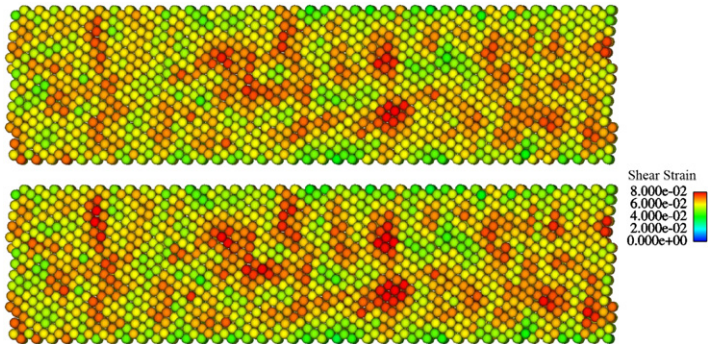

Figure 6. Computed Almansi (top) and Green (bottom) strains at 6.0% applied strain.

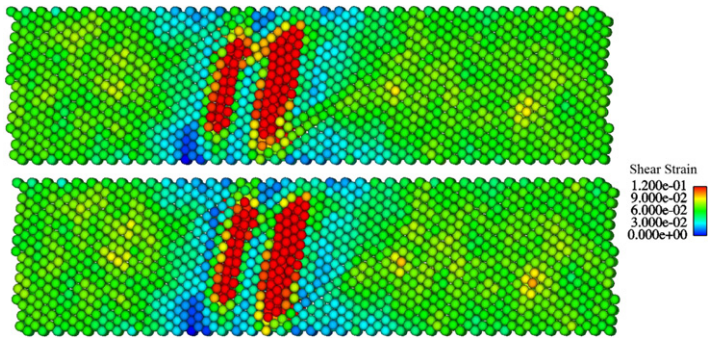

Figure 7. Computed Almansi (top) and Green (bottom) strains at 6.4% applied strain.

in the post-plastic flow regime. In particular, the Almansi strain shows most shear activity along the $(\bar{1}\,1\,1)$ slip plane, while the Green strain shows most activity along the $(1\,1\,1)$ planes. This difference is accounted for by considering the orientation of the active slip systems. For example, the relative motion along adjacent $(1\,1\,1)$ slip planes can be approximated locally by simple shear. The corresponding Almansi strain is

$$\varepsilon^* = \frac{1}{2}\begin{bmatrix} 0 & k & 0 \\ k & -k^2 & 0 \\ 0 & 0 & 0 \end{bmatrix}, \tag{31}$$

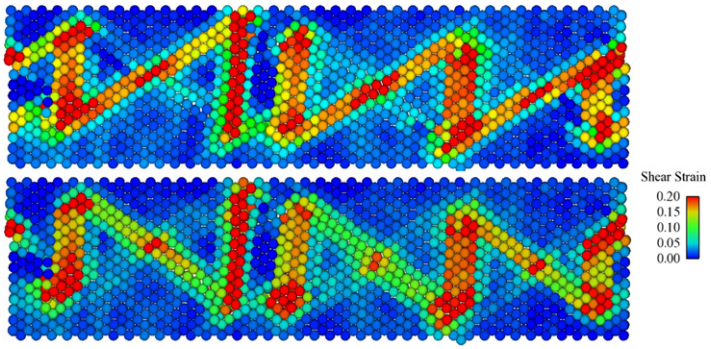

Figure 8. Computed Almansi (top) and Green (bottom) strains at 7.0% applied strain.

in which ε^* is expressed in terms of a local coordinate system with x^* oriented along the direction of slip. The parameter k is the ratio of slip to spacing of adjacent slip planes. Expressing ε^* in terms of the global x and y directions yields the following Almansi shear strain component

$$\varepsilon_{12} = -\tfrac{1}{4}k(-2\cos 2\theta + k\sin 2\theta) \tag{32}$$

in which θ is the angle between x and x^*. The Green shear strain component is

$$E_{12} = \tfrac{1}{4}k(2\cos 2\theta + k\sin 2\theta), \tag{33}$$

and the difference between the Almansi and Green strain is

$$E_{12} - \varepsilon_{12} = k^2(\cos\theta\sin\theta). \tag{34}$$

Thus, the Green and Almansi shear values will be equivalent for (1 0 0) slip and differ for (1 1 1) and ($\bar{1}$ 1 1) slip. As a particular example, at 7% applied strain, $k \simeq 0.6$. The corresponding Green and Almansi shear strain along (1 1 1) are $E_{12} = 0.02$ and $\varepsilon_{12} = 0.19$, while values along ($\bar{1}$ 1 1) are $E_{12} = 0.19$ and $\varepsilon_{12} = 0.02$. These values closely correspond to the computed Almansi and Green strain results in figure 8. This result allows interpretation of the post yield bulk average Almansi and Green shear results in figure 3. In particular, the bulk Almansi being larger than the Green indicates that more slip is occurring on the (1 1 1) planes than on the ($\bar{1}$ 1 1).

2.2. Local atomic strains

To examine the local strain computations at individual atoms, we compare the computed results for atoms 764 and 2129 with positions indicated in figure 9. Atom 764 is located in a region below the active slip plains, while atom 2129 is subject to significant slip activity. The computed shear strain time histories for these atoms are shown in figures 9(*b*) and 9(*c*). Until the localization of strain occurs at 6.4% applied strain, the magnitudes of the computed strains match those of the the applied strain. After localization the computed strain rates correspond with the applied strain rate, but the magnitudes do not.

Atom 764 lies in a region of homogeneous and elastic deformation. The computed strain history follows a cyclic loading and unloading. During the loading cycles, the strain increases at a rate consistent with the applied strain rate. The local strain is then partially or completely relieved at a much higher rate due to localization of the strain along the slip planes. Atom 2129 is located in a region of significant inhomogeneous deformation, and the strain history follows a somewhat different pattern from that of atom 764. Instead of relaxing at the maximum

stress, the strain jumps from 7.6% to 17.6%, followed by a linear increase in strain at a rate equal to the applied strain rate. At 8% applied strain, the strain relaxes from 18% to 14%. This decrease is then followed by a steady increase in computed strain and a jump at 14% applied strain from 21% to 25%. One observes that the jumps in strain at both atoms occur at the same applied strains, and that the strain at the atom in the elastic region decreased while the strain at the atom in the slip plane increased.

2.3. Weight function effects on computed strain

The relevant length scale for the atomic strain examined by changing both the weight function form and cutoff radius. The bulk average computed shear strains using three different weight functions are plotted in figure 10. The weight functions used in computing the atomic Green strains were: a Heaviside step function in which all atoms within a cutoff radius were given a weight of 1.0, a cubic spline as shown in figure 2(*a*), and the multi-step function shown in 2(*b*). When considering the weight function form, the cutoff radius was fixed at 8 Å resulting in a total of approximately 200 atoms contributing to the deformation gradient optimization. When examining the cutoff radius the size varied from 4 to 10 Å.

During homogeneous deformation, the weight function has little effect on the computed strains with specific values varying from the applied strain by less than 1.0%. Once plastic flow begins, the magnitude of the computed strains exhibits some sensitivity, with the results using the Heaviside and cubic spline functions being closest to the applied strain.

Strains computed using the Heaviside function follow the applied strain more closely than those computed from the cubic or step function. After a jump from 1% to 2% at the transition from homogeneous to inhomogeneous deformation, the difference from the applied strain decreases to approximately 1.2%. The strains computed using the cubic and step functions, which are more sensitive to motion of the nearest neighbors, show a small but more pronounced deviation from the applied strain. The cubic jumps from 0.7% to 2.0% difference and increases to approximately 3.0%, and the step function jumps from 0.4% to 3.8% and increases to 4.0% over the course of the deformation.

The choice of weight function impacts the strain tensor calculation primarily through increasing or decreasing contribution of remote neighbors. For the Heaviside function, this results in a suppression of the effects of local slip because atoms within the 8 Å cutoff radius but outside the 4 Å wide slip bands make significant contributions to the local strain calculations, thus, yielding a result closer to the homogeneous applied strain. With the multi-step function, the primary contributions to the formation of the deformation gradient come the first and second nearest neighbors. In this case, the effect of shear along the crystallographic slip planes is locally pronounced and manifest through bulk Green shear strains that are smaller than the applied shear strains.

To directly examine the effect of weight function radius, the Almansi shear strains were computed for atom 2129 using the functions shown in figure 2(*b*), and the results are plotted in figure 11. By increasing the cutoff radius, additional atoms are considered in determination of the local strain. With a cutoff radius of 4 Å, 12 neighbors contribute to the strain. A cutoff of 6 Å adds a contribution of six additional neighbors, and so on.

The range of the weight function cutoff radii considered here includes the 5.65 Å cutoff radius used for the energy potential. Varying the size of the strain cutoff radius independently from the energy cutoff radius, facilitated examination of the relevant length scale for calculation of strain. In this example, figure 10, the local variations in the computed strain arise due to localized slip. While differences arise in various locations, volume average Green strain shows

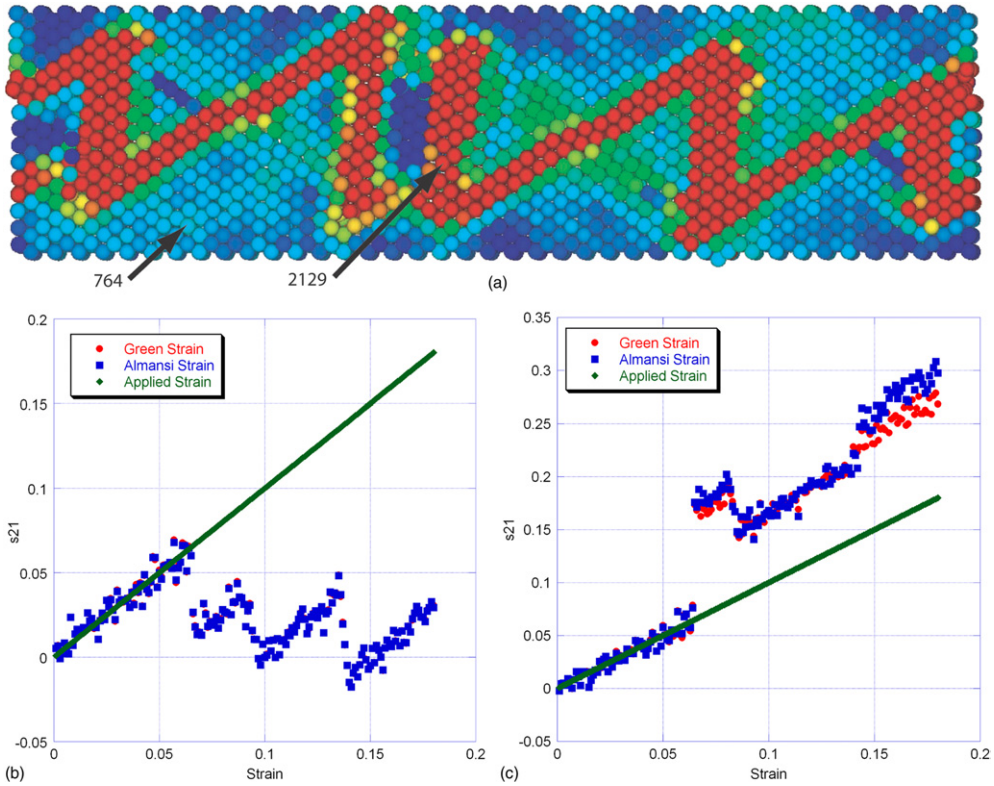

Figure 9. Computed Green and Almansi strain at atoms 764 and 2912. The computed strains are provided for atoms 764 and 2129. Atom 764 is in a region of small relative displacements among its neighbors while atom 2129 is in a region in which significant amounts of slip occur.

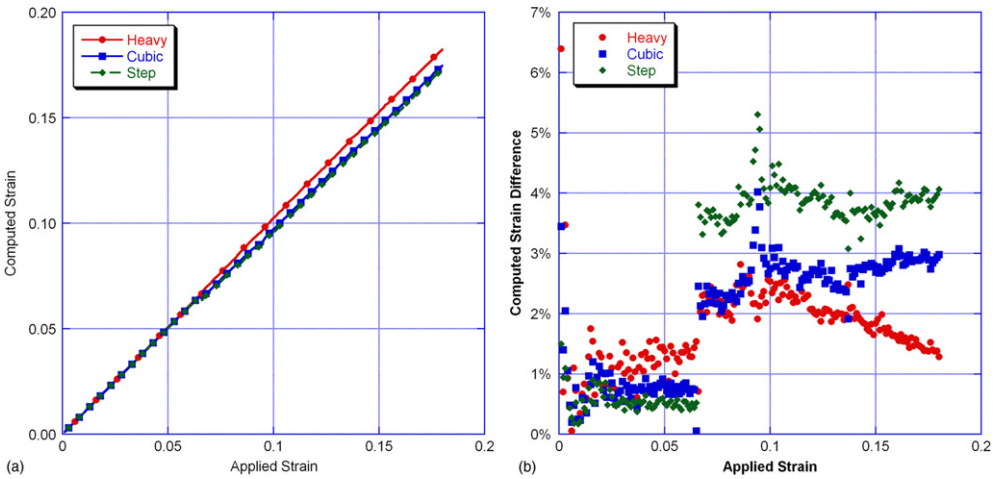

Figure 10. Bulk average computed shear strains using Heaviside, cubic and multi-step functions; (*a*) shows the average computed Green strains and (*b*) shows the per cent difference between the computed Green and applied strains.

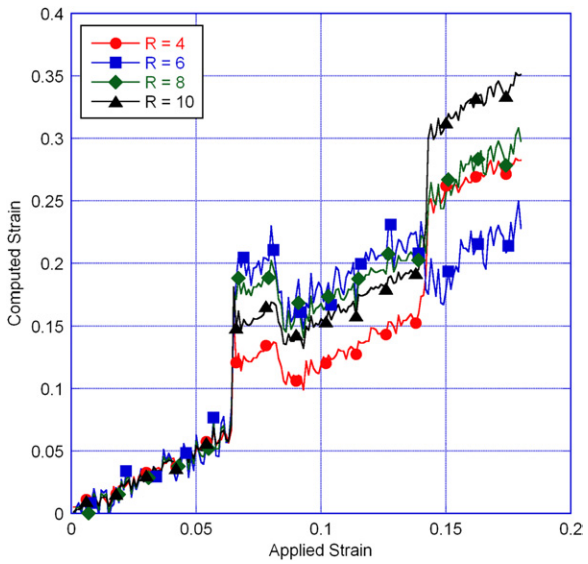

Figure 11. Computed Almansi strain at Atom 2129 using various cutoff radii, R.

minimal variation. Volume average Almansi strains may exhibit significant differences for 4 and 6 Å cutoff radii and minimal variation for 8 and 10 Å radii.

As expected, computed strains were independent of cutoff radius during homogeneous deformation. After 6.4% applied strain, the computed strains follow a similar pattern, but the strain magnitudes vary with cutoff radius size. At 6.4% applied strain, the computed strains all exhibit a jump, with magnitudes ranging from 6.6% for a cutoff of 4 Å to 12.9% for a radius of 6 Å. At approximately 8.4% applied strain, the computed strains relax. The strain computed considering only nearest neighbors (4 Å) decreases to within 2% of the applied shear curve, while the others indicate slightly higher shear levels. The next jump in the local strain occurs at 14% applied strain. Here the 4 Å strain jumps to the same value as the 8 Å measure, while the 6 Å drops to the applied strain level. The largest jump occurs for the 10 Å case which approaches a level of 30%. With this cutoff radius, significant contributions are made from atoms as far as 6 Å which includes atoms at the bottom of the sample that are subject to the largest magnitudes of slip. Although the results at atom 2129 are sensitive to cutoff radii in this range, this effect is primarily due to the relative size of the slip region compared with the cutoff radius and the complexity and variation of the slip directions and magnitudes in the region. For regions in which slip is more uniform in magnitude and direction among neighbors, e.g. at atom 764, the variation of computed strain does not exhibit similar jumps.

3. Conclusions

A new approach for computing a deformation gradient from discrete atomic data has been presented. The motivation for this algorithm was to develop a means of computing finite deformation strain tensors from discrete atomic simulation data that correspond to continuum strain tensors. The proposed deformation gradient emerges from a weighed least squares optimization of local deformation data and may be used to compute strain or other deformation-related quantities.

The computations for the proposed formulation utilize position vectors and neighbor lists from atomistic simulations to compute a deformation gradient. The computational complexity of the algorithm, excluding the generation of neighbor lists, scales linearly with the number of atoms, i.e. O(N). Once the deformation gradient is constructed, any desired strain tensor may be computed. In contrast, strain tensors relying on geometric decompositions of interatomic regions, such as a Delaunay triangulation of atomic sites in $\mathbb{R}^3$, will require approximately O($N \log N$), e.g. see [16] or [17].

The simulation of simple shearing of an atomic slab was performed to evaluate the computed strain values of the proposed method. The results demonstrate the consistency between the computed atomic strains and continuum finite deformation strain predictions. For homogeneous deformations, the strain values were shown to be computed precisely, and rotations properly accounted for. Although other methods for computing strain are available, e.g. [9], the advantage of the proposed method is that finite strains and rotations can be resolved correctly when based on the deformation gradient. This is not true for methods based on small-strain definitions. In those methods even relatively small rotations will result in incorrect strain values. Thus, the finite strain model is better suited for establishing cause-effect relations for incorporation into macroscale models.

The computed shear strains in regions of localization are sensitive to the weighting of distant neighbors through either the choice of weight function and/or the size of cutoff radius used. The effect of localization on the computed bulk strains becomes less apparent as the effective size of the cutoff zone is increased. The sensitivity of the local atomic strain to the size of the cutoff radius appears to decrease when the size of the localization increases relative to the local atomic region.

Acknowledgments

This work was sponsored by Mississippi State University Center for Advanced Vehicular Systems and by the US Department of Energy under Contract No W-7405-ENG-36.

References

[1] Liu W K, Karpov E G, Zhang S and Park H S 2004 An introduction to computational nanomechanics and materials *Comput. Methods Appl. Mech. Eng.* **193** 1529–78

[2] Tadmor E B, Ortiz M and Phillips R 1996 Quasicontinuum analysis of defects in solids *Phil. Mag.* A **73** 1529–63 (Engl. Transl.)

[3] Horstemeyer M F, Baskes M I, Prantil V C, Philliber J and Vonderheide S 2003 A multiscale analysis of fixed-end simple shear using molecular dynamics, crystal plasticity, and a macroscopic internal state variable theory *Modelling Simul. Mater. Sci. Eng.* **11** 265–86 (Engl. Transl.)

[4] Horstemeyer M F, Baskes M I and Plimpton S J 2001 Length scale and time scale effects on the plastic flow of fcc metals *Acta Mater.* **49** 4363–74

[5] Kelchner C L, Plimpton S J and Hamilton J C 1998 Dislocation nucleation and defect structure during surface indentation *Phys. Rev.* B **58** 11085–8 (Engl. Transl.)

[6] Zimmerman J A, Kelchner C L, Klein P A, Hamilton J C and Foiles S M 2001 Surface step effects on nanoindentation *Phys. Rev.* B **87** 165507/1-4 (Engl. Transl.)

[7] Mott P H, Argon A S and Suter U W 1992 The atomic strain tensor *J. Comput. Phys.* **101** 140–50

[8] Ward D K, Curtin W A and Qi Y 2006 Mechanical behavior of aluminum-silicon nanocomposites: a molecular dynamics study *Acta Mater.* **54** 4441–51

[9] Falk M L 1999 Molecular-dynamics study of ductile and brittle fracture in model noncrystalline solids *Phys. Rev.* B **60** 7062–70

[10] Horstemeyer M F and Baskes M I 1999 A strain tensor and other kinematic quantities at the atomic scale *Multiscale Phenomena in Materials* vol 578 (Boston, MA: Materials Research Society)

[11] Hirth J P and Lothe J 1967 *Theory of Dislocations* (*McGraw-Hill Series in Materials Science and Engineering*) (New York: McGraw-Hill)
[12] Ogden R W 1984 *Non-Linear Elastic Deformations* (New York: Dover)
[13] Daw M S and Baskes M I 1984 Embedded-atom method: derivation and application to impurities, surfaces, and other defects in metals *Phys. Rev.* B **29** 6443–53
[14] Daw M S, Foiles S M and Baskes M I 1993 The embedded-atom method: a review of theory and applications *Mater. Sci. Rep.* **9** 251–310 ((c) 2002 Inst. For Sci. Info.)
[15] Born M and Huang K 1988 *Dynamical Theory of Crystal Lattices* (*Oxford Classic Texts in the Physical Sciences)* (Oxford: Clarendon/Oxford University)
[16] Devillers O, Meiser S and Teillaud M 1992 Fully dynamic delaunay triangulation in logarithmic expected time per operation *Comput. Geom.* **2** 55–80
[17] Barber C B, Dobkin D P and Huhdanpaa H 1996 The quickhull algorithm for convex hulls *ACM Trans. Math. Softw.* **22** 469–83